



HAL
open science

Chemical and physical transfers in an ultramafic rock weathering profile: 2. Dissolution vs. accumulation of platinum group minerals

Daouda Traoré, Anicet Beauvais, Thierry Augé, Jean Claude Parisot, Fabrice Colin, Michel Cathelineau

► To cite this version:

Daouda Traoré, Anicet Beauvais, Thierry Augé, Jean Claude Parisot, Fabrice Colin, et al.. Chemical and physical transfers in an ultramafic rock weathering profile: 2. Dissolution vs. accumulation of platinum group minerals. *The American Mineralogist*, 2008, 93, pp.31-38. 10.2138/am.2008.2606 . hal-01422041

HAL Id: hal-01422041

<https://amu.hal.science/hal-01422041>

Submitted on 23 Dec 2016

HAL is a multi-disciplinary open access archive for the deposit and dissemination of scientific research documents, whether they are published or not. The documents may come from teaching and research institutions in France or abroad, or from public or private research centers.

L'archive ouverte pluridisciplinaire **HAL**, est destinée au dépôt et à la diffusion de documents scientifiques de niveau recherche, publiés ou non, émanant des établissements d'enseignement et de recherche français ou étrangers, des laboratoires publics ou privés.

1 **Revision 1 (including editorial corrections)**

2
3 **Chemical and physical transfers in an ultramafic rock weathering profile: 2. Dissolution**
4 **vs. accumulation of platinum group minerals**

5
6 Daouda Traoré ^{1,2}, Anicet Beauvais ^{1,2,*}, Thierry Augé³, Jean Claude Parisot ^{1,2},

7 Fabrice Colin ^{1,2}, Michel Cathelineau ⁴

8
9 ¹ *Institut de Recherche pour le Développement (IRD), UMR 161 CEREGE, BP A5, 98848*

10 *Nouméa, Nouvelle-Calédonie*

11 ² *Centre Européen de Recherche et d'Enseignement des Géosciences de l'Environnement,*
12 *(UMR IRD 161), Aix-Marseille Université, Université Paul Cézanne, B.P. 80, 13545 Aix-en-*

13 *Provence Cedex 4, France*

14
15 ³ *Bureau de Recherche Géologique et Minière, B.P. 6009, 45060 Orléans Cedex 2, France*

16
17 ⁴ *UMR G2R/CREGU Université Henri Poincaré 54506 Vandoeuvre-lès-Nancy, France*

18
19
20
21
22
23
24
25
26 *Corresponding author: Anicet.beauvais@noumea.ird.nc (Tel/Fax: (687) 26 07 59/67)

27

27

ABSTRACT

28

29

30

31

32

33

34

35

36

37

38

39

40

41

42

43

44

45

46

The chemical weathering of ultramafic rocks has resulted in eluvial concentration of platinum-group minerals (PGM) in lateritic weathering profiles of southern New Caledonia. The Pt mineralization interpreted as being primary consists of platinum-group minerals included in chromite crystals. The occurrence of PGM as free particles in the weathering profile results from the supergene dissolution of Pt-bearing chromite (Traore et al. 2007). Following their release in the profile, supergene dissolution processes variably affect the PGM particles. The behavior of platinum-group elements in the weathering profile is characterized by significant loss of Pd and relative accumulation of Pt indicating that Pd is more mobile than Pt in the exogenous cycle. Unstable Pt-Fe-Cu-Pd alloys and PGE oxides undergo chemical and mineralogical changes to acquire the chemical configuration of the isoferroplatinum (Pt_3Fe), which is the most stable Pt-phase in a lateritic environment. The isoferroplatinum phase may also be dispersed throughout the weathering mantle and/or accumulated in the lower parts of profiles according to a translocation mechanism of residual Pt-rich fine particles driven by percolation of water through the connected pore spaces.

Keywords: Platinum group minerals, platinum group elements, lateritic weathering, ultramafic rocks, New Caledonia.

46

INTRODUCTION

47

48

49

50

51

52

53

54

55

56

57

58

59

60

61

62

63

64

65

66

67

68

69

70

Lateritic weathering processes affect numerous regions of the intertropical zone (Pedro 1968; Nahon 1986; Tardy and Roquin 1992), where long term chemical weathering has led to the supergene accumulation of metals in profiles of 10 to 100 meters in thickness, and among them, precious metals such as Au and Pt. Previous studies concerning the behavior of Au and Pt have proven useful for tracing the geochemical evolution of lateritic weathering covers within which they are concentrated (Colin et al. 1993, 1997; Varajao et al. 2000).

Although hypotheses about the chemical mobilization of platinum-group elements (PGE) under supergene conditions are not new (Wagner 1929), the platinum-group minerals (PGM) are generally considered as resistant phases during weathering (Cabri and Harris 1975; Hattori and Cabri 1992). Much controversy remains, however, about the mobility of PGE, i.e., the geochemical and physical processes controlling their redistribution as PGM partial dissolution versus neo-formation processes in the surface-weathering environment. For example, Augustithis (1965) hypothesized the supergene formation of PGM in lateritic weathering materials from ultramafic rocks of Ethiopia. Two years later, Otteman et al. (1967) suggested that PGM formed during hydrothermal serpentinization. Over the last decades, numerous field and geochemical studies have shown the solubility of PGE in supergene environments (Bowles 1986; Middleworth and Wood 1999; Varajao et al. 2000; Azaroual et al. 2001; Oberthür et al. 2003). We investigate the geochemical behavior of the PGE and the physical-chemical processes controlling the PGM mineralogy under the influence of supergene conditions in a lateritic weathering profile from New Caledonia to characterize the dissolution and/or the accumulation of those minerals.

Previous studies at this site have shown that a lateritic mantle has developed at the expense of the primary mineralization and that it is systematically characterized by higher Pt and Pd

71 contents than the bedrock (Augé et al. 1995). The most common PGM identified in the
72 secondary mineralization are the Pt minerals, mainly isoferroplatinum, Pt₃Fe, which
73 represents about 60 percent of PGM (Augé and Legendre 1994). The other major alloys
74 identified are tulameenite (Pt₂FeCu) and tetraferroplatinum (PtFe). Accessory cooperite and
75 Rh-Ir-Pt-Fe oxides were also found (Augé and Legendre 1994). Previous studies at other
76 sites have shown that PGM were, for the most part, included in chromite crystals (Augé
77 and Maurizot 1995). A detailed mineralogical and micro chemical study of the PGM
78 present in the weathering profile may be useful to characterize the physical and
79 geochemical processes underlying the evolution of this profile.

80 **GEOLOGICAL AND GEOMORPHOLOGICAL SETTING**

81 The Pirogues River dunite-gabbro unit of the New Caledonian Southern Massif (Fig.
82 1) exhibits stratiform chromite-bearing rocks containing PGE at the base of a cumulate
83 series. A lateritic weathering mantle is developed at the expense of the platinum
84 mineralization under the influence of a warm and humid climate, which is characterized
85 by a mean annual rainfall of 1700 mm with a wet season occurring from December to
86 August, and a mean annual temperature of 22°C (Jaffré 1980).

87 The Pirogues River PGE mineralization (Fig. 1) is specifically related to chromitite in
88 pyroxenite dikes crosscutting the basal ultramafic cumulate series, and in rare cases in
89 decimetric scale chromite schlierens in the host wehrlite (Augé and Maurizot 1995).
90 Chromitite occurs in the dikes as many local decimeter to meter scale segregations. Chromite-
91 free facies are not mineralized in PGE. Platinum-group elements (Pt dominant) take the form
92 of PGM that are, for the most part, included in chromite crystals (Augé and Maurizot 1995).
93 The parent rock underwent strong lateritic weathering processes that has led to the dissolution
94 of chromite, and thus, to the release of platinum-group minerals in the weathering mantle

95 (Traore et al. 2007). Previous studies have also shown a contrast in behavior between the
96 PGE and chromite in the lateritic mineralization (Augé et al. 1995).

97 Natural weathering profiles exposed in deep gullies incising hillslopes. One of these
98 profiles (also locally called “lavakas”) has been described and sampled *in situ* (Fig. 2a) for a
99 thorough study of the PGM released in the weathering matrices. A companion paper
100 addresses the mineralogical and geochemical nature of the profile (Traore et al. 2007). The
101 weathering profile is developed from a wehrlite type ultramafic rock, and its thickness
102 (to 4 m) has been divided into four main layers (Fig. 2a). At the base of the profile, the
103 greenish-black parent rock changes to the brownish coarse saprolite that preserves the
104 structure and the texture of bedrock. The mineralogical characterization indicates
105 olivine, antigorite, diopside and goethite, with accessory chromite and enstatite. The
106 coarse saprolite is progressively transformed into a fine saprolite, in which the texture and the
107 structure of the parent rock are still preserved. The chromite grains are progressively
108 dissolved that results in the depletion of chromium and the release of PGM (Traore et al.
109 2007). At the top of the fine saprolite, the silicates are completely weathered into goethite.
110 Toward the top of the profile, the fine saprolite changes to reddish laterites in which the
111 original rock structures are no longer preserved. The mineral assemblage is dominated by
112 goethite, with accessory hematite and chromite.

113 MATERIAL AND METHODS

114 Fourteen samples of parent rock, laterite and soil were crushed and finely ground.
115 According to the PGM-MS23 analytical procedure developed by the Australian Laboratory
116 Services (ALS, Chemex), each prepared sample was fused with a mixture of lead oxide,
117 sodium carbonate, borax and silica, inquarted with 6 mg of gold-free silver and then cupelled
118 to yield a precious metal bead. The bead was digested for 2 minutes at high power by
119 microwave in dilute nitric acid. The solution was cooled and hydrochloric acid was added.

120 The solution was digested for an additional 2 minutes at half power by microwave. The
121 digested solution was then cooled, diluted to 4 ml with 2 % hydrochloric acid, homogenized
122 and then analyzed for platinum and palladium by inductively coupled plasma – mass
123 spectrometry (ICP-MS). Detection limits for Pd and Pt are 1 and 0.5 ppb, respectively.

124 Five hundred particles of PGM were extracted from three samples (1 sample = 50 kg) in
125 different parts of the profiles (fine saprolite, mottled zone and nodular layer), before being
126 examined by scanning electron microscopy (SEM) for morphological analysis, and by
127 electron microprobe for micro-chemical analysis.

128 The samples were damped in a 20-liter drum, and then put in a concrete mixer to
129 disaggregate the non-indurated nodules. The remaining non-indurated nodules were manually
130 crushed and the resulting mix was sifted to 1 mm for eliminating fragments of rock and
131 ferricrete prior to sorting with an automatic pan to separate out the heaviest particles. For each
132 sample, heavy-mineral concentrates were separated into three grain-size fractions ($< 65 \mu\text{m}$,
133 $65\text{-}200 \mu\text{m}$ and $> 200 \mu\text{m}$). Platinum-group mineral grains were isolated from the other heavy
134 minerals. Because the PGM size ranges between 10 and $40 \mu\text{m}$ (Augé and Legendre 1994;
135 Augé and Maurizot 1995), the particle morphologies of the smaller grain-size fractions (< 65
136 μm) were directly examined using SEM. The fraction between 65 and $200 \mu\text{m}$ was separated
137 with a hand magnet into ferromagnetic and para- and non-magnetic fractions. The collected
138 PGM grains were mounted on aluminum stubs for SEM morphoscopic examination and EDS
139 semi-quantitative analysis.

140 Micro-chemical analyses of the PGM were made using a Cameca SX 50 electron
141 microprobe under multiple analytical conditions in a single run. The analytical procedure was
142 designed for routine analysis of PGM (Augé and Legendre 1992) including the quantitative
143 analysis of oxygen. The analytical conditions (except for O) included an acceleration voltage
144 of 25 keV, a beam current of 20 nA, and counting time of 6 s. The standards used are Cr_2O_3

145 for Cr, AsGa for As, pyrite for Fe and S, stibnite for Sb, and pure metals for all other
146 elements. The X-ray lines used were $K\alpha$ for Ni, Cu, Cr and Mn, $K\beta$ for Fe, $L\alpha$ for Rh, Ir, Pt,
147 and Ru, and $L\beta$ for Os, Pd, and As. Oxygen was analyzed using the $K\alpha$ line with an
148 acceleration voltage of 10 kV. The change of acceleration voltage was made automatically
149 during the analytical cycle. The Cameca PAP correction program was used.

150 **RESULTS AND DISCUSSION**

151 **Chemical and physical characterization of PGE and PGM**

152 **PGE bulk chemistry.** Figure 2 shows the variation of Pt and Pd contents and of
153 the Pt/Pd ratio along the profile. Palladium concentration significantly increases in the
154 upper fine saprolite (Fig. 2b), while Pt reaches a maximum of $647 \mu\text{g.kg}^{-1}$ in the coarse
155 saprolite, with a mean value of $512 \mu\text{g.kg}^{-1}$ in the fine saprolite and decreases to 240
156 $\mu\text{g.kg}^{-1}$ in the mottled zone and to $196 \mu\text{g.kg}^{-1}$ in the soft nodular layer (Fig. 2c). The
157 Pt/Pd ratio increases from 14 in the fresh wehrlite to 29 in the coarse saprolite, and
158 decreases to 14 in the fine saprolite and to 10 in the mottled zone and soft nodular layer
159 (Fig. 2d).

160 Although the absolute concentrations of Pt and Pd may not be directly comparable between
161 the weathered profile and the parent rock, the increase of Pt/Pd ratio from the fresh rock to
162 the saprolite and to the mottled zone (soft nodular layer being mostly a material transported
163 mechanically on the hillslope) suggests that Pd is more mobile than Pt and dispersed
164 chemically in the supergene environment (Fuchs and Rose 1974; Evans et al. 1994;
165 Prichard and Lord 1994; Oberthür et al. 2003).

166 **PGM distribution and micro morphology.** Platinum-group metal distribution in the
167 weathering profile is heterogeneous. Ninety five percent of the collected particles are in the
168 fine saprolite, 4% in the mottled zone and only 1% in the nodular layer. Although the residual
169 PGM particles present in the lateritic weathering profiles have various shapes and surface

170 aspects, the examination of PGM under electronic microscope allows for differentiation of
171 three main morphological groups (Fig. 3). Euhedral PGM particles, with smooth surfaces and
172 perfect crystal faces (Fig. 3a) are the least abundant and they are only found in the fine
173 saprolite and the mottled zone. Rounded PGM particles are found in the fine saprolite and the
174 mottled zone. Their crystal edges are smooth and their surfaces exhibit micrometric cracks
175 and/or etching pits (Fig. 3b). The roughest PGM particles (Fig. 3c) were collected in the soft
176 nodular layer and are strongly weathered. They have also been found in the fine
177 saprolite and the mottled zone.. The size of etching pits on those particles increases from
178 the lower to the upper horizons of the profile.

179 **Physical vs. chemical weathering signatures of PGM micromorphology.** The
180 heterogeneous PGM distribution in the weathering profile and the significant concentration of
181 round and rough PGM particles in the fine saprolite horizon can be explained by mechanical
182 transfer and accumulation similar to the vertical translocation of small gold particles through
183 relatively large porosity and higher groundwater hydrodynamic conditions (Michel 1987;
184 Butt 1987; Colin et al. 1993; Hanlie 2000).

185 The size and shape of the cavities and/or etching pits in the PGM particles suggest that
186 they result from a dissolution process. Deep in the saprolite, the pits are round and small; their
187 sizes gradually increased upward in the weathering profile.

188 An additional change in PGM micromorphology consists of increasing rounding upward,
189 from the saprolite to the soil surface. The rounding is most obvious in the mottled zone (Fig.
190 3b) and soft nodular layer (Fig. 3c). The absence of striations and impact marks precludes
191 smoothing by a transport mechanism. The roundness is therefore attributed entirely to a
192 dissolution process.

193 The large cracks affecting the grains of PGM are interpreted to be a result of a change in
194 volume due to chemical leaching in the oxidizing environment (Augé and Legendre 1994;

195 Oberthür et al. 2003). Our observations support this interpretation but the composite grains
196 exhibit differential weathering patterns according to the PGM types. The Pt-Fe-(Cu-Pd) alloys
197 and PGE oxides are effectively more weathered than isoferroplatinum in the lateritic
198 weathering profiles as shown by microchemical analyses and SEM photographs (Figs. 4 and
199 5).

200 **PGM micro chemical analysis.** Platinum-group elements of the Pirogues River lateritic
201 mineralization zones are associated with platinum-iron alloys and oxides. A nomenclature of
202 the PGM is proposed, based on their chemical composition and previous works (Augé and
203 Legendre 1994; Augé and Maurizot 1995). Three species of PGM recognized are
204 isoferroplatinum (Pt_3Fe) that represents the majority of the PGM studied, and undetermined
205 Pt-Fe-(Cu-Pd) alloys and PGE-oxides. See Tables 1 and 2 in the *American Mineralogist*
206 *Online Background Dataset* for the microchemical composition of the different species of
207 PGM.

208 The microchemical composition of isoferroplatinum is shown in Figure 4. Its Pt content
209 varies between 58 and 69 at.%; Fe content ranges between 21 and 26 at.%; and Pd varies only
210 from 0.2 to 2.7 at.%. While Cu does not enter in significant amounts into the isoferroplatinum
211 composition, its content ranges from 0.2 to 4 at.%. The isoferroplatinum generally occurs as
212 euhedral or subhedral grains (Fig. 5a), which are chemically homogeneous and form free
213 particles, or is associated with other PGM (Fig. 5b and 5c). They may also constitute
214 weathered rims around porous and rough particles (Fig. 6d).

215 The undetermined Pt-Fe-(Cu-Pd) alloys form euhedral and subhedral grains, and are
216 sometimes characterized by an internal structure with concentric zoning (Fig. 6a). Another
217 morphological type of the Pt-Fe-(Cu) system is a symplectic intergrowth with a phase that has
218 not been preserved (Fig. 6b and 6c). The grains are isolated or associated with
219 isoferroplatinum and/or PGM oxides in composite particles (Fig. 5b). Their reflectance is

220 lower than that of the isoferroplatinum. In many cases, the Pt-Fe-(Cu) grains present large
221 cracks and/or weathered rims.

222 Microprobe analyses of Pt-Fe-(Cu) particles indicate a relatively wide range of
223 compositions (Fig. 4). Platinum contents vary from 38 to 50 at.%; Fe from 20 to 28 wt.%; Pd
224 from 1 to 12 at.%; and Cu from 12 to 26 at.%.

225 The existence of PGE-oxides has been widely established (Legendre and Augé 1993;
226 Prichard and Lord 1994; Augé and Legendre 1994; Augé and Maurizot 1995; Jedwab 1995;
227 Salpeteur et al. 1995; Garuti et al. 1997; Moreno et al. 1999; Hey, 1999; Oberthür et al. 2003).
228 Platinum-group elements oxides are exceptionally abundant in the Pirogues River area where
229 they form subhedral or rounded grains, which appear chemically heterogeneous (Fig. 7 and
230 8). The oxidized compounds of PGE are associated with the other PGM in composites
231 particles, or form free particles in the lateritic weathering profiles. Their reflectance is
232 significantly lower than that of isoferroplatinum, and slightly lower than that of Pt-Fe-(Cu-Pd)
233 alloys as shown in Figure 5b. PGE oxide particles are often cracked and/or present weathered
234 rims (Fig. 5c and 6d).

235 Based on microprobe analyses, two compositional types of PGE oxides can be distinguished:

236 (1) Pt-Fe (Cu-Pd) oxides with Pt contents varying between 20 at.% and 46 at.%; Fe varies
237 from 16 at.% to 30 at.%; Pd from 0 to 7 at.%; and Cu varies from 0 to 10 at.%. Representative
238 analyses of the grains including oxygen are given in Figure 7. Oxygen contents indicate a
239 relatively wide compositional range from 16 to 61 at.%, but with a relatively constant atomic
240 ratio of (Pt+Pd)/(Fe+Cu).

241 (2) Rh-Ir-Pt-Fe oxides constitute small grains associated with Pt-Fe alloys and/or other
242 PGE oxides (Fig. 5b, and 5c). Their main chemical components are Rh (12 to 36 at.%; Pt (0
243 to 18 at.%; Ir (0 to 3 at.%; Fe (11 to 53 at.%; Pd (0 to 9 at.%). The oxygen content varies
244 from 14 to 51 at. % (Fig. 8).

245 Detailed electron microprobe profiles have been performed on specific PGE oxides grains.
246 The porous core of grain PGB7_4h shows the presence of S (up to 12 at.%) (Fig. 9). The rest
247 of the grains show significant amount of Si and Mg with 0.2 to 4 at.% and traces of Pd.

248 The frequent association of a PGE alloy and a PGE oxide suggests that the oxide does not
249 derive from the Pt-Fe alloy. The systematic amount of S in the oxide (Fig. 9), though minor,
250 suggests that the oxide could have been derived from a sulfide. A serpentinization process
251 could have led to the desulfurization of primary PGE sulfides and contributed to the formation
252 of an unstable oxidized phase (Stockman and Hlava 1984; Garuti and Zaccarini 1997). It is
253 very likely that oxidation occurs at an early stage, as oxides are abundant in weakly weathered
254 chromitite.

255 **Selective dissolution of PGM**

256 The rough PGM grains exhibit weathering rims developed around a primary mineral.
257 This is particularly evident in PGE oxides as well as for the undetermined Pt-Fe-(Cu-Pd)
258 alloys, which can exhibit a weathered cortex that appears silver-white and porous on the SEM
259 and backscattered electron imaging (Fig. 10). Microprobe analyses from the core to the
260 weathered edge indicate a significant compositional change. The weathered rim has lower Cu
261 content, which varies on average from 18.51 at. % in the core to 6.98 at. % in the weathered
262 zone. Iron decreases on average from 23.32 at. % for the parent PGM to 19.96 at. % for the
263 weathered external part. Platinum is relatively enriched and increases from 47.7 at. % to 68.18
264 at. % from the core to the weathered edges of the grains. Palladium varies from 0.88 at. % in
265 the core to 0.3 at. % in the weathered rim (Fig. 10).

266 **Isoferroplatinum accumulation**

267 The Pt-Fe-(Cu-Pd) alloys and PGE oxides affected by the weathering process develop
268 weathering rims, which are depleted in Cu, Pd and Fe, and relatively enriched in Pt. These Pt-
269 minerals are thus impoverished in Cu, Pd and Fe and tend to acquire the chemical

270 composition of isoferroplatinum (Pt_3Fe), which is a more stable mineralogical phase in the
271 supergene environment. The weathered particles have generally preserved both the structure
272 and the chemical signature (in the core of the grains) of the fresh PGM particles (Fig. 10).

273 This clearly demonstrates that the PGM particles are residual but are affected by dissolution.

274 The evidence of a supergene accumulation of isoferroplatinum is not new. Several field
275 studies have reported the formation of Pt-Fe alloys of isoferroplatinum type from pre-existing
276 unstable PGM under low-temperature conditions (Cousins and Kinloch 1976; Evans et al.
277 1994; Salpeteur et al. 1995; Oberthür et al. 2003). Our observations indicate also that
278 mineralogical changes occur in the supergene environment by the transformation of unstable
279 PGM to porous and friable grains enriched in platinum as isoferroplatinum small particles that
280 can be mechanically redistributed in the lateritic weathering profiles. Our results further
281 indicate that Pt is dispersed mainly in particulate form by mechanical processes, whereas Pd
282 is released mainly in solution (Wood and Vlassopoulos 1990; Cook and Fletcher 1994;
283 Prichard and Lord 1994; Evans et al. 1994; Oberthür et al. 2003).

284

CONCLUSION

285 An eluvial concentration of platinum-group minerals was studied in a lateritic
286 weathering profile, which developed at the expense of ultramafic rocks in southern New
287 Caledonia. The PGE in the weathering profile take the form of PGM, which are mostly
288 concentrated in the fine saprolite horizon. Our study confirms the abundance of PGE oxides
289 in the Pirogues mineralized system and shows that they can derive from desulfurization of
290 pre-existing PGE sulfides. Our results demonstrate that the PGE alloys of the Pt-Fe-(Cu)
291 system and PGE oxides are weathered in a supergene environment. These PGM undergo
292 selective partial dissolution according to a chemical eluviation gradient ($\text{S} > \text{Cu} > \text{Pd} > \text{Fe} >$
293 Pt) that leads to the formation of richer Pt-phases such as Pt_3Fe . The resulting
294 isoferroplatinum grains are relatively stable regarding the supergene dissolution processes and

295 mostly transferred mechanically through the connected porosity lower in the weathering
296 profiles, where they accumulate in a cementation zone.

297

ACKNOWLEDGEMENTS

298 This work is a contribution IRD-UMR161-CEREGE. Dr. P. Maurizot is thanked for
299 introducing us to the study area. J. Butscher, D. Chardon, V. Chevillotte, V. Combier, A.
300 Paugam, J. Perrier, N. Perrier and B. Robineau are thanked for their help during fieldwork.
301 Dr. Giorgio Garuti and Dr. Anthony Velbel are gratefully acknowledged for their stimulating
302 reviews of the manuscript.
303

REFERENCES CITED

- 303
304 Augé, T., and Legendre, O. (1992) Pt-Fe nuggets from alluvial deposits in eastern
305 Madagascar. *Canadian Mineralogist*, 30, 983-1004.
- 306 Augé, T., and Legendre, O. (1994) Platinum-group element oxides from the Pirogues
307 ophiolitic mineralization, New Caledonia: Origin and Significance. *Economic Geology*,
308 89, 1454-1468.
- 309 Augé, T., and Maurizot, P. (1995) Stratiform and alluvial platinum mineralization in the New
310 Caledonia ophiolite complex. *Canadian Mineralogist*, 33, 1023-1045.
- 311 Augé, T., Maurizot, P., Breton, J., Eberlé, J.M., Gilles, C., Jézéquel, P., Mézière, J., and
312 Robert, M. (1995) Magmatic and supergene platinum-group minerals in the New
313 Caledonia ophiolite. *Chronique de la Recherche Minière*, 520, 3-26.
- 314 Augustithis, S.S. (1965) Mineralogical and geochemical studies of the platiniferous dunite-
315 birbire-pyroxénite complex of Yubdo, Birnir, West Ethiopia. *Chemie der*
316 *Erde/Geochemistry*, 24, 159-165.
- 317 Azaroual, M., Romand, B., Freyssinet, P., and Disnar, J. (2001) Solubility of platinum in
318 aqueous solutions at 25°C and pHs 4 to 10 under oxidizing conditions. *Geochimica et*
319 *Cosmochimica Acta*, 65, 4453-4466.
- 320 Bowles, J.F.W. (1986) The development of platinum-group minerals in laterites. *Economic*
321 *Geology*, 81, 1278-1285.
- 322 Butt, C.R.M. (1987) A basis for geochemical exploration models for tropical terrains.
323 *Chemical Geology*, 60, 5-16.
- 324 Cabri, L.J., and Harris, D.C. (1975) Zoning in Os-Ir alloys and the relation of the geological
325 and tectonic environment of the source rocks to the bulk Pt: Pt+Ir+Os ratio for placers.
326 *Canadian Mineralogist*, 13, 266-274.

- 327 Colin, F., Sanfo, Z., Brown, E., Bourlès, D., and Minko, A.E. (1997) Gold: a tracer of the
328 dynamics of tropical laterites. *Geology*, 25, 81-84.
- 329 Colin, F., Veillard, P., and Ambrosi, J.P. (1993). Quantitative approach to physical and
330 chemical gold mobility in equatorial rainforest lateritic environment. *Earth and Planetary
331 Science Letters*, 114, 269-285.
- 332 Cook, S.J., and Fletcher, W.K. (1994) Platinum distribution in soil profiles of the Tulameen
333 ultramafic complex, southern British Columbia. *Journal of Geochemical Exploration*, 51,
334 161-191.
- 335 Cousins, C.A., and Kinloch, E.D. (1976) Some observations on textures and inclusions.
336 *Economic Geology*, 71, 1377-1393.
- 337 Evans, D.M., Buchanan, D.L., and Hall, G.E.M. (1994) Dispersion of platinum, palladium
338 and gold from the Main Sulphide Zone, Great Dike, Zimbabwe. *Transactions of the
339 Institution of Mining and Metallurgy*, 103, (Section B: Applied earth science), B57-B67.
- 340 Fuchs, W.A., and Rose, A.W. (1974) The geochemical behavior of platinum and palladium in
341 the weathering cycle in the Sillwater complex, Montana. *Economic Geology*, 69, 332-346.
- 342 Garuti, G., and Zaccarini, F. (1997) *In situ* alteration of platinum-group-minerals at low
343 temperature: evidence from serpentized and weathered chromitite of the Vourinos
344 complex, Greece. *Canadian Mineralogist*, 35, 611-626.
- 345 Garuti, G., Zaccarini, F., Cabella, R., and Fershtater, G. (1997) Occurrence of unknown Ru-
346 Os-Ir-Fe oxides in the chromitites of the Nurali Ultramafic complex, Southern Urals,
347 Russia. *Canadian Mineralogist*, 35, 1431-1439.
- 348 Hanlie, H. (2000) Behaviour of gold in the weathered mantle at Shewushan, Hubei, China.
349 *Journal of Geochemical Exploration*, 68, 57-68.
- 350 Hattori, K., and Cabri, L.J. (1992) Origin of platinum-group-mineral nuggets inferred from an
351 Osmium-Isotope study. *Canadian Mineralogist*, 30, 289-301.

- 352 Hey, P.V. (1999) The effects of weathering on the UG2 Chromitite reef of the Bushveld
353 complex, with special reference to the platinum-group minerals. South African Journal of
354 Geology, 102, 251-260.
- 355 Jaffré, T. (1980) Végétation des roches ultrabasiques en Nouvelle-Calédonie. Travaux et
356 Documents, 275 p., ORSTOM 124, Paris, France.
- 357 Jedwab, J. (1995) Oxygenated platinum-group-element and transition-metal (Ti, Cr, Mn, Fe,
358 Co, Ni) compounds in the supergene domain. Chronique de la Recherche Minière, 520, 47-
359 53.
- 360 Legendre, O., and Augé, T. (1993) Présence d'un oxyde d'iridium naturel dans les
361 concentrations platinifères de la région d'Antambao-Manampotsy, Madagascar. Comptes
362 Rendus de l'Académie des Sciences, série II, 316, 921-927.
- 363 Michel, D. (1987) Concentration of gold in *in situ* laterites from Mato Grosso. Mineralium
364 Deposita, 22, 185-189.
- 365 Middlesworth, J.M.V., and Wood, S.A. (1999) The stability of palladium (II) hydroxide and
366 hydroxy-chloride complexes: An experimental solubility study at 25-85°C and 1 bar.
367 Geochimica et Cosmochimica Acta, 63, 1751-1765.
- 368 Moreno, T., Prichard, M.H., Lunar, R., Monterrubio, S., and Fisher, P. (1999) Formation of a
369 secondary platinum-group mineral assemblage in chromitites from the Herbeira ultramafic
370 massif in Cabo Ortegal, NW Spain. European Journal of Mineralogy, 11, 363-378.
- 371 Nahon, D.B. (1986) Evolution of iron crusts in tropical landscapes. In S.H. Coleman, and
372 D.P. Dethier, Eds., Rates of Chemical Weathering of Rocks and Minerals, p. 169-187.
373 Academic Press Inc., San Diego.
- 374 Oberthür, T., Weiser, T.W., and Gast, L. (2003) Geochemistry and mineralogy of platinum-
375 group elements at Hartley Platinum Mine, Zimbabwe. Mineralium Deposita, 38, 344-355.

- 376 Otteman, J., and Augustithis, S. S. (1967) geochemistry and origin of "platinum-nugget" in
377 lateritic covers from ultrabasic rocks and birbirites of West Ethiopia. *Mineralium Deposita*,
378 1, 269-277.
- 379 Pedro, G. (1968) Distribution des principaux type d'altération chimique à la surface du globe.
380 Présentation d'une esquisse géographique. *Revue de Géographie Physique et Géologie*
381 *Dynamique*, 10, 457-470.
- 382 Prichard, M.H., and Lord R.A. (1994) Evidence for differential mobility of platinum-group
383 elements in the secondary environnement in Shetland ophiolite complex. *Transactions of*
384 *the Institution of Mining and Metallurgy*, 103, (Section B; Applied earth science), B79-
385 B86.
- 386 Salpeteur, I., Martel-Jantin, B., and Rakotomanana, D. (1995) Pt and Pd mobility in ferralitic
387 soils of the west Andramana area (Madagascar). Evidence of a supergene origin of some Pt
388 and Pd minerals. *Chronique de la Recherche Minière*, 520, 27-46.
- 389 Stockman, H.W., and Hlava, P.F. (1984) Platinum-group minerals in Alpine chromitites from
390 Southwestern Oregon. *Economic Geology*, 79, 491-508.
- 391 Tardy, Y., and Roquin, C. (1992) Geochemistry and evolution of lateritic landscapes. In I.P.
392 Martini, and W.Chesworth, Eds., *Weathering, Soils & Paleosols*, p. 407-443. Elsevier
393 Publishing, Amsterdam.
- 394 Traoré, D., Beauvais, A., Augé, T., Chabaux, F., Peiffert, C., Parisot, J.C., Ambrosi, J.P., and
395 Colin, F. (2007) Chemical and physical transfers in an ultramafic rock weathering profile:
396 1. Dissolution of Pt-bearing chromite. *American Mineralogist*, submitted.
- 397 Varajao, C.A.C., Colin, F., Vieillard, P., Melfi, A.J., and Nahon, D. (2000) Early Weathering
398 of palladium gold under lateritic conditions, Maquine Mine, Minas Gerais: Brazil. *Applied*
399 *Geochemistry*, 15, 245-263.

- 400 Wagner, P.A. (1929) The platinum deposits and mines of South Africa, 326 p. Oliver and
401 Boyd, Edinburgh.
- 402 Wood, S.A., and Vlassopoulos, D. (1990) The Dispersion of Pt, Pd, and Au in surficial media
403 about two PGE-Cu-Ni prospects in Quebec. *Canadian Mineralogist*, 28, 649-663.
- 404

404 **Figures Caption**

405

406 Figure 1. (a) geological map and location of studied area (after Augé and Maurizot, 1995).

407 The black star shows the location of the studied weathering profile (Fig. 2). (b) Inset of the

408 main Island of New Caledonia with its ultramafic massifs and location of (a) by the black

409 rectangle.

410

411 Figure 2. (a) Description of the weathered profile from a crosscut in a natural gully

412 (“lavaka”) and the location of studied samples (white squares). Vertical variations of contents

413 of (b) Pd, (c) Pt and of (d) ratio Pt/Pd along that profile are illustrated.

414

415 Figure 3. SEM photomicrographs of PGM grains with (a) euhedral, (b) smooth and (c) rough

416 morphologies.

417

418 Figure 4. Compositional variations in the Pt-Fe-Cu system of isoferroplatinum (black circles),

419 tetraferroplatinum (grey circles) and tulameenite (black stars). The analyses are plotted as

420 atomic percent (at%).

421

422 Figure 5. SEM photomicrographs of (a) automorphous isoferroplatinum, (b) composite PGM

423 of Pt-Fe-Pd alloy (light grey), isoferroplatinum (white) and Rh-Fe oxide (dark grey), and (c)

424 composite particle of isoferroplatinum (white), Rh-Fe oxide (dark grey) and Pt-Fe oxide.

425

426 Figure 6. SEM photomicrographs of (a) euhedral zoned Pt-Fe alloy, (b) and (c) symplectic

427 PGM composite grain, (d) PGM grain with weathering rim.

428

429 Figure 7. Compositional variation of Pt-Fe(Cu-Pd) oxides. The analyses are plotted as atomic

430 percent (at%).

431

432 Figure 8. Compositional variation of Rh-Ir-Pt-Fe oxides shown in Figures 5b and 5c. The
433 analyses are plotted as atomic percent (at%).

434

435 Figure 9. Compositional variation through (a) a zoned particle with a porous core. The
436 numbers represent the spot microanalyses given in (b). Light grey hexagons = Pt, black
437 triangles = Fe, black circles = O, grey squares = S, and (c) grey triangles = Mg, light grey
438 stars = Pd and black diamonds = Si.

439

440 Figure 10. Compositional variation from (a) a Pt-Fe-Cu alloy (light grey core) to a secondary
441 isoferroplatinum (white rim). The numbers represent the spot microanalyses given in (b).

442 Light hexagons = Pt, light grey triangles = Fe, black circles = Cu and light grey stars = Pd.

443

444

445 **Table captions (for depository)**

446 TABLE 1. Microchemical composition of isoferroplatinum, tetraferroplatinum and
447 tulameenite.

448

449 TABLE 2. Microchemical composition of platinum oxides.

450

451

452

453

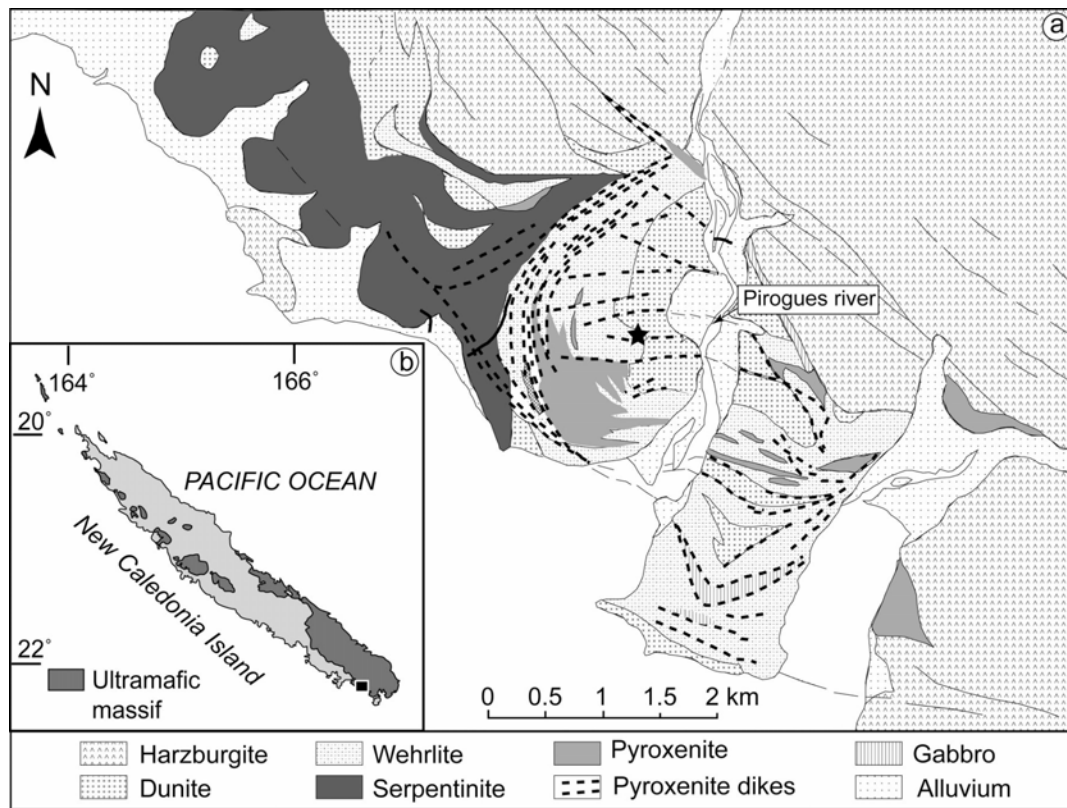


FIG. 1

454

Traore et al., 2007

455

456

457

458

459

460

461

462

463

464

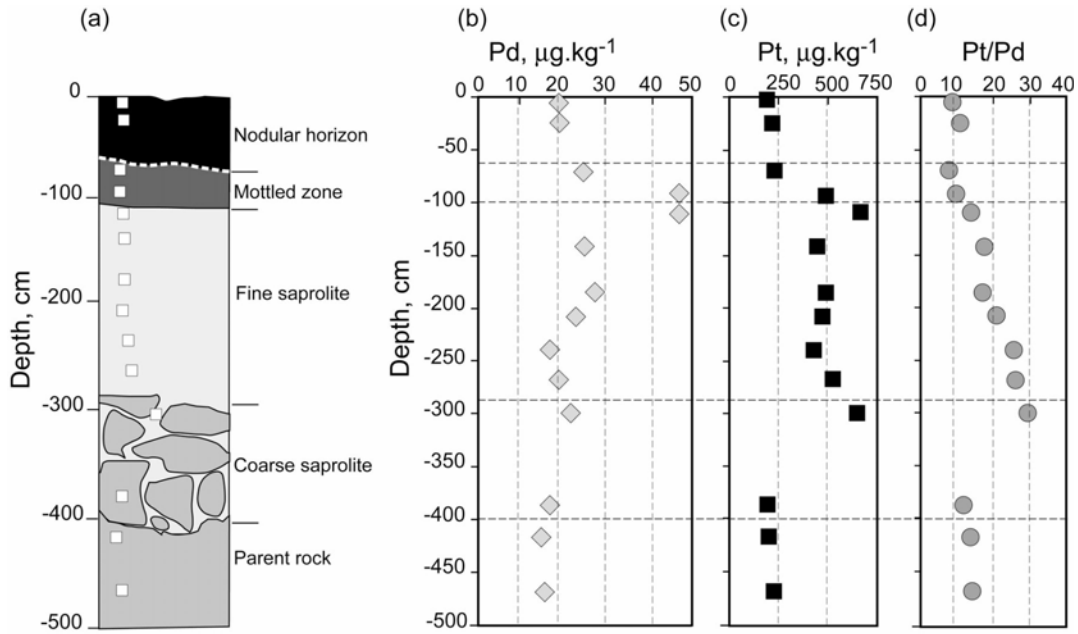


FIG. 2

465

Traore et al., 2007

466

467

468

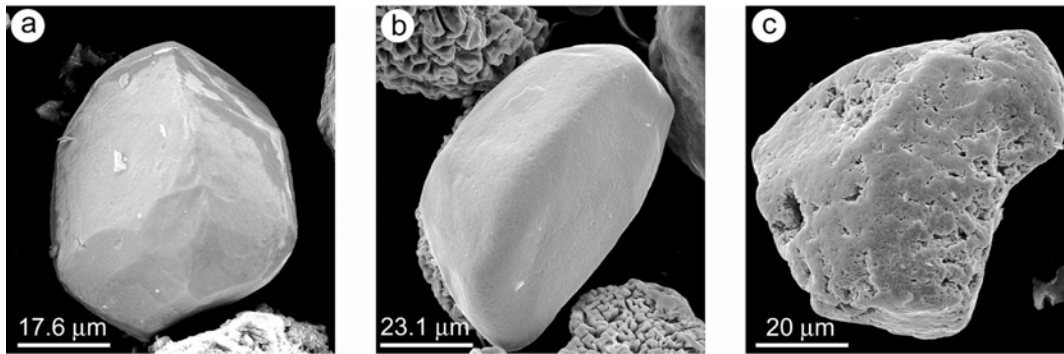


FIG. 3

469

Traore et al., 2007

470

471

471

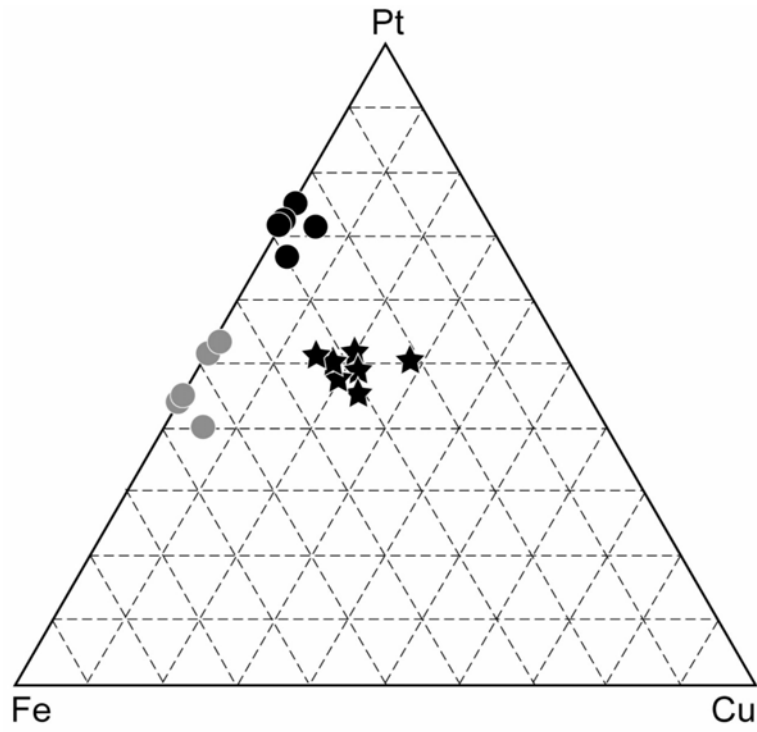


FIG. 4

Traore et al., 2007

472

473

474

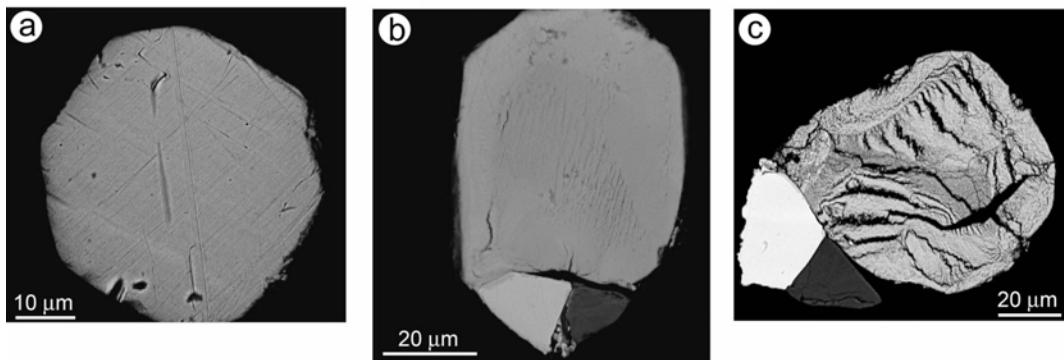


FIG. 5

475

Traore et al., 2007

Traore et al., 2007

476

477

478

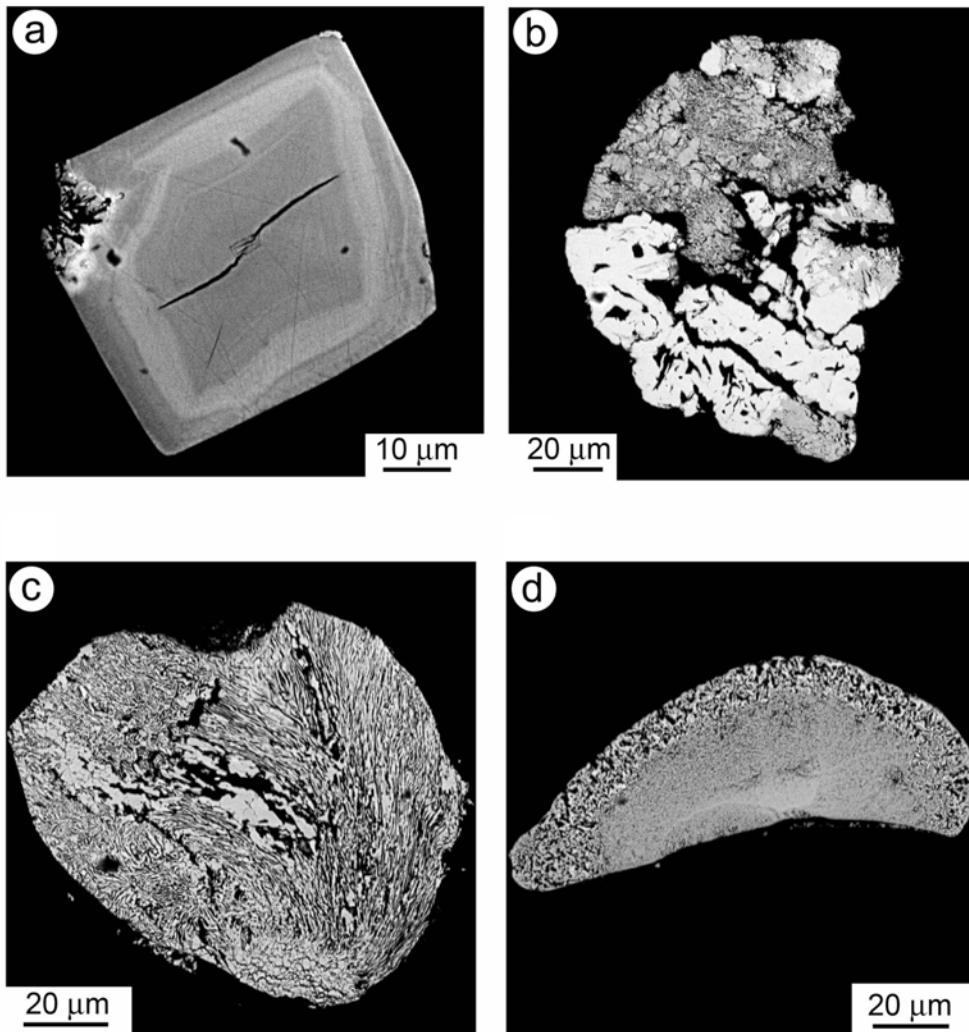


FIG. 6

479

Traore et al., 2007

480

481

482

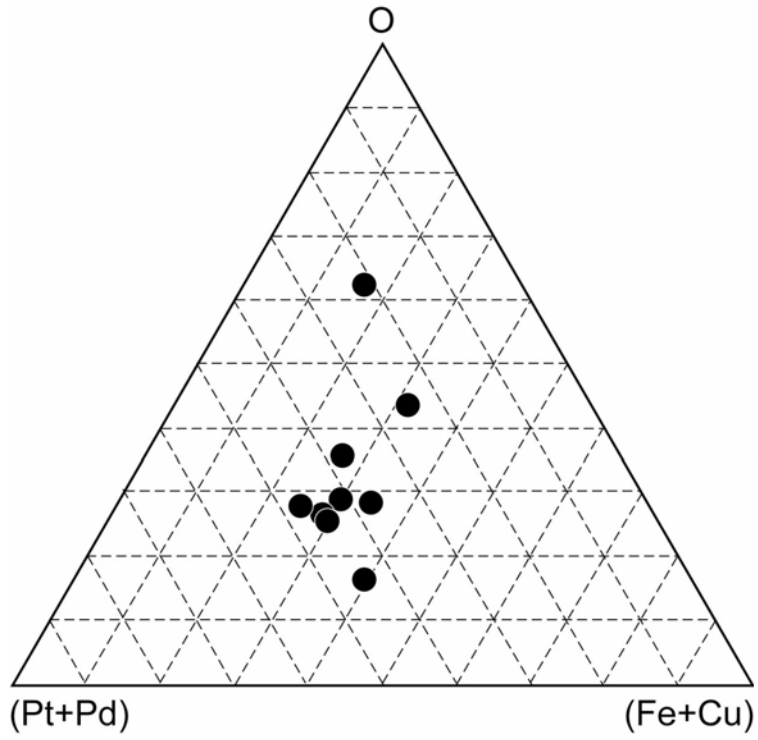


FIG. 7

483

Traore et al., 2007

484

485

486

487

488

489

490

491

492

493

494

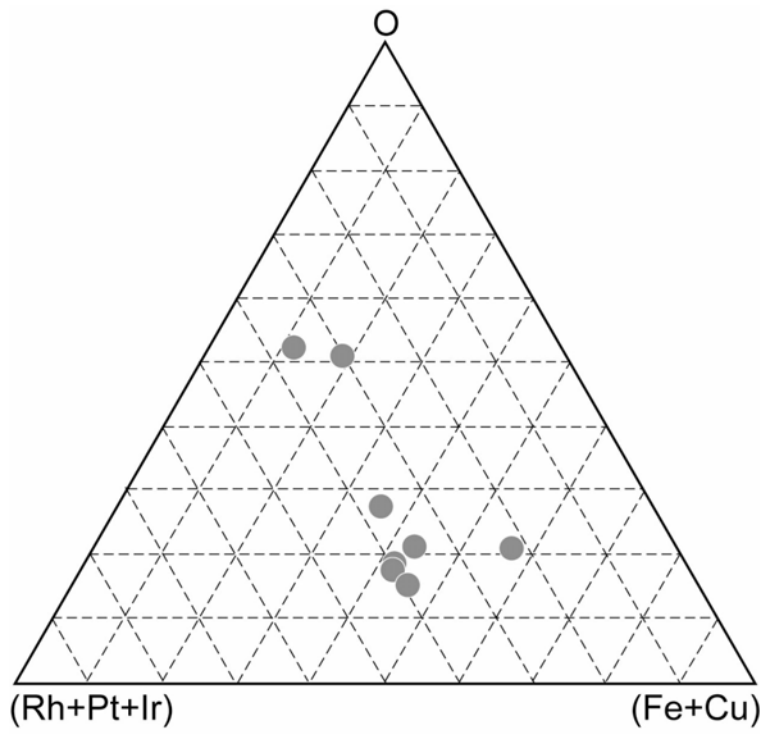


FIG. 8

Traore et al., 2007

495

496

497

498

499

500

501

502

503

504

505

506

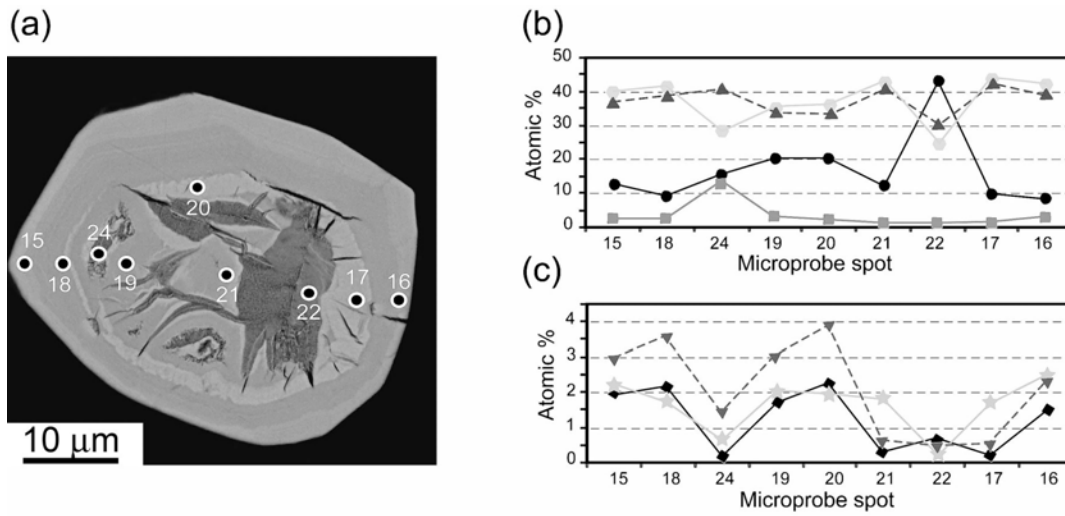


FIG. 9

507

Traore et al., 2007

508

509

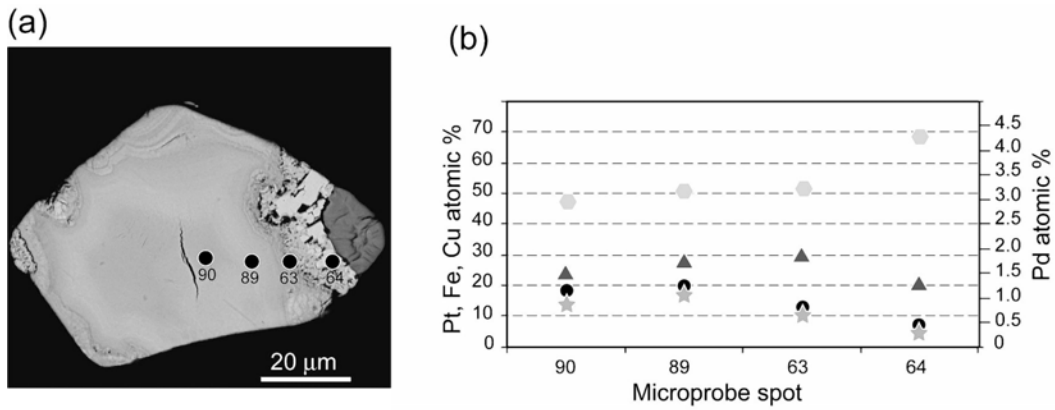


FIG. 10

Traore et al., 2007

510

Traore et al., 2007

Isoferroplatinum Pt ₃ Fe							Pt-Fe-(Cu) system												
							Tetraferroplatinum Pt-Fe					Tulameenite Pt-Fe-Cu							
Sample n°	PGB1_13	PGB1_16b	PGB7_8b	PGB7_8a	PGB7_13n	PGB6_19a	PGB1_5a	PGB1_16b	PGB7_13m	PGB5_1	PGB5_1	PGB1_6	PGB1_7a	PGB5_6	PGB5_6	PGB5_8	PGB7_7b	PGB5_8	
Atomic percent																			
Pt	65.45	65.26	69.43	58.26	64.29	65.97	44.31	47.02	37.99	39.27	38.88	41.71	38.10	38.88	40.33	42.85	50.60	47.00	
S	0.26	0.23	0.00	0.13	0.46	0.12	0.31	0.02	2.99	2.41	2.76	0.29	0.15	0.25	0.19	0.15	0.21	0.19	
Fe	25.08	24.91	22.92	26.47	21.51	21.39	41.66	40.21	50.61	48.09	48.03	27.94	24.76	26.78	27.82	26.52	27.27	20.32	
Pd	2.74	2.33	0.20	2.70	1.82	2.38	1.35	1.49	1.50	0.55	0.75	6.90	6.15	12.07	11.18	8.64	1.09	2.76	
As	0.00	0.08	0.00	0.00	0.05	0.18	0.00	0.23	0.00	0.00	0.00	0.18	0.10	0.00	0.20	0.05	0.00	0.07	
Ni	0.00	0.24	0.00	0.79	0.43	0.14	0.55	1.45	0.05	0.22	0.10	0.22	0.31	0.80	0.92	0.66	0.86	1.17	
Cu	0.22	0.18	0.72	3.69	4.04	0.75	0.64	1.63	0.06	0.00	0.13	12.60	14.86	20.23	17.74	20.48	19.06	26.23	
Co	0.00	0.00	0.00	0.00	0.00	0.00	0.08	0.23	0.00	0.00	0.00	0.08	0.00	0.00	0.00	0.00	0.00	0.00	
Ir	0.11	0.00	0.37	0.09	0.18	0.22	0.40	0.11	0.00	0.22	0.01	0.12	0.18	0.05	0.00	0.00	0.10	0.03	
Cr	0.00	0.00	0.00	0.12	0.35	0.16	0.05	0.04	0.03	0.06	0.00	0.11	0.06	0.19	0.14	0.02	0.00	0.06	
Rh	0.39	0.43	1.19	0.32	0.46	0.75	0.28	0.30	0.38	0.31	0.20	0.76	0.28	0.15	0.02	0.51	0.48	0.42	
O	5.76	6.32	5.00	7.42	6.40	7.70	9.82	7.13	5.84	8.59	8.77	8.95	14.76	0.55	1.29	0.06	0.18	1.71	
Si	0.00	0.01	0.12	0.00	0.00	0.09	0.22	0.13	0.00	0.06	0.02	0.02	0.19	0.02	0.03	0.06	0.10	0.03	
Mg	0.00	0.00	0.00	0.00	0.00	0.09	0.32	0.02	0.54	0.23	0.35	0.13	0.10	0.02	0.03	0.00	0.00	0.00	
Mn	0.00	0.00	0.00	0.00	0.00	0.08	0.00	0.00	0.03	0.01	0.00	0.00	0.00	0.00	0.09	0.00	0.03	0.00	
Total	100.00	100.00	100.00	100.00	100.00	100.00	100.00	100.00	100.00	100.00	100.00	100.00	100.00	100.00	100.00	100.00	100.00	100.00	

TABLE 1

Traore et al., 2007

Sample n°	(Pt-Pd)-Fe oxides						Pt-(Fe-Cu) oxides			(Rh-Ir-Pt)-(Fe-Cu) oxides								
	PGB1_8c	PGB1_9a	PGB1_16	PGB1_16e	PGB1_16a	PGB7_4h	PGB7_1	PGB4_1	PGB4_2a	PGB7_7b	PGB5_1	PGB6_8a	PGB5_8	PGB5_9	PGB6_19a	PGB6_19a	PGB1_9a	
Atomic percent																		
Pt	38.57	31.74	38.78	37.90	20.94	24.50	46.47	35.29	41.86	18.45	7.14	14.65	0.25	0.43	0.37	0.47	0.13	
S	0.07	0.18	0.25	0.18	0.03	0.54	0.01	0.17	0.32	0.50	2.46	0.87	0.39	0.42	1.00	0.06	1.35	
Fe	28.95	26.46	29.38	28.16	16.67	29.98	17.59	27.55	28.49	11.65	53.61	18.47	35.12	32.19	41.97	39.76	32.77	
Pd	5.39	5.64	1.41	6.73	0.64	0.26	0.44	0.86	1.26	0.00	0.09	0.03	5.74	9.58	0.23	0.88	0.03	
As	0.00	0.00	0.15	0.00	0.05	0.00	0.00	0.00	0.06	0.04	0.00	0.00	0.00	0.02	0.00	0.00	0.00	
Ni	0.23	0.03	0.24	0.11	0.06	0.06	0.11	1.98	0.49	0.20	0.00	0.10	0.04	0.00	0.00	0.02	0.03	
Cu	0.04	0.00	0.00	0.00	0.00	0.29	6.97	6.34	9.99	0.16	0.10	0.37	4.85	5.42	0.25	0.41	0.05	
Co	0.01	0.00	0.14	0.00	0.01	0.00	0.00	0.00	0.00	0.00	0.00	0.00	0.00	0.00	0.00	0.00	0.05	
Ir	0.00	0.06	0.00	0.16	0.00	0.14	0.09	0.00	0.07	2.59	2.64	0.49	0.30	0.37	2.06	1.80	1.16	
Cr	0.06	0.00	0.03	0.00	0.13	0.03	0.06	0.07	0.01	0.40	0.00	0.46	0.00	0.00	0.14	0.16	0.10	
Rh	0.19	0.20	0.18	0.09	0.08	0.26	0.54	0.19	0.26	14.26	11.89	14.20	36.08	33.96	34.41	31.45	32.02	
O	25.95	35.36	28.80	26.14	61.03	42.84	27.43	27.29	16.00	51.11	20.95	49.88	17.16	17.46	14.67	20.46	25.71	
Si	0.48	0.06	0.63	0.32	0.31	0.59	0.16	0.26	0.15	0.23	0.44	0.15	0.02	0.04	1.96	1.84	2.41	
Mg	0.06	0.03	0.00	0.00	0.00	0.42	0.08	0.00	0.16	0.22	0.61	0.23	0.03	0.11	2.95	2.70	4.20	
Mn	0.00	0.26	0.00	0.20	0.04	0.04	0.00	0.00	0.85	0.18	0.05	0.11	0.00	0.00	0.00	0.00	0.00	
Total	100.00	100.00	100.00	100.00	100.00	100.00	100.00	100.00	100.00	100.00	100.00	100.00	100.00	100.00	100.00	100.00	100.00	

TABLE 2.

Traore et al., 2007